Quantifying primary oxidation products in the OH-initiated reaction of benzyl alcohol

Reina S. Buenconsejo[1], Sophia M. Charan[1], John H. Seinfeld[1], and Paul O. Wennberg[1]

[1]California Institute of Technology, Pasadena, CA 91125

Correspondence: Paul O. Wennberg (wennberg@caltech.edu)

Abstract. Benzyl alcohol is found in many volatile chemical products (VCPs) including a number of personal care products and industrial solvents. We report here the products of the gas-phase oxidation of benzyl alcohol by OH and its dependence on nitric oxide (NO) levels. Using gas chromatography (GC) in tandem with chemical ionization mass spectrometry (CIMS) and gas chromatography with a flame ionization detector (GC-FID), we measure the branching fractions to the major gas-phase oxidation products, hydroxybenzyl alcohol (HBA) and benzaldehyde. Later-generation oxidation products from both HBA and benzaldehyde pathways are also observed. In particular, catechol is a major gas-phase product of HBA. The fraction of H-abstraction from benzyl alcohol leading to benzaldehyde formation is unaffected by [NO], with an average branching fraction of $(21 \pm 10)\%$. The fraction of OH addition leading to HBA formation $(36 \pm 18)\%$ also does not appear to vary with [NO]. Consistent with the known high SOA yields of catechol, we find that HBA has a very high secondary organic aerosol (SOA) yield. Thus, benzyl alcohol and its oxidation products efficiently produce secondary organic aerosol—under some conditions approaching unity. Insights from the present study can help elucidate the chemistry of other atmospherically-relevant aromatic compounds, especially those found in VCPs.

1 Introduction

Emissions of volatile chemical products (VCPs) have been recently identified as critical in driving air pollution chemistry, particularly as regulations drive a decrease in the contribution of vehicular-based emissions (McDonald et al., 2018; Coggon et al., 2021). VCPs play an important role in air quality because of their high potential to form secondary organic aerosol (SOA); an analysis of VCPs in the Los Angeles Air Basin indicates that VCPs could contribute up to 70% of SOA formation in the Los Angeles Air Basin despite accounting for only approximately 4% of total petrochemical product use (McDonald et al., 2018). The inclusion of VCP emission inventories has improved the agreement of regional scale modeling compared to previous models that did not consider VCP emissions (Seltzer et al., 2021; Pennington et al., 2021). However, because many of the chemicals comprising VCP emissions have not been studied in laboratory settings, their contribution to SOA formation ~~is uncertain. Therefore, additional~~ remains uncertain. Additional experimental work on VCPs is still needed.

Here, we evaluate the photochemistry of benzyl alcohol, a compound found prominently in VCPs. Benzyl alcohol is used in soaps and perfumes, and is also used as a solvent in the manufacture of paints, inks, lacquers, and epoxies (Wang, 2015). In a

previous study, the aerosol mass yield of benzyl alcohol was found to have a high mass yield under a variety of conditions—even approaching unity (Charan et al., 2020; Jaoui et al., 2023).

Experimental studies, including kinetic experiments on benzyl alcohol, have determined that the primary atmospheric oxidative pathway of benzyl alcohol proceeds via reaction with the ~~OH~~ hydroxyl radical (OH) radical (Bernard et al., 2013; Harrison and Wells, 2009). Harrison et al. calculated that benzyl alcohol reacts with OH at a rate of $(28 \pm 7) \times 10^{-12}$ $cm^3 molecule^{-1}s^{-1}$. The reaction rate with O_3 is too slow to ~~signficantly~~ significantly affect to benzyl alcohol mixing ratios in most environments (Harrison and Wells, 2009).

Previous experimental studies of benzyl alcohol identified several oxidation products including hydroxybenzyl alcohol (HBA) and benzaldehyde (Burkholder et al., 2017; Harrison and Wells, 2009; Bernard et al., 2013). A theoretical study on the mechanism of benzyl alcohol oxidation initiated by ~~hydroxy radicals (OH)~~ OH also predicted the major oxidation pathways form benzaldehyde, i-hydroxybenzyl alcohol, and o-hydroxybenzyl alcohol (Wang, 2015). Other products observed in past experimental studies include ring-opening products, such as but-2-enedial and 6-hydroxy-5-oxohex-2-enal (Harrison and Wells, 2009), as well as C6 compounds such as dihydroxy benzene (Bernard et al., 2013). These past experiments were conducted under high NO conditions. Yet, understanding chemical mechanisms and branching fractions as a function of NO is important for understanding the impact of its oxidation on urban air quality as NO_x to VOC ratios have been shown to affect OH oxidation of VOCs and as NO_x regimes continue to change in urban settings (Seinfeld and Pandis, 2016; Parker et al., 2020). This is particularly relevant as NO_x continues to decline in many U.S. urban areas (Parker et al., 2020).

In this study, we draw on past work which suggests HBA forms via addition of OH to the benzyl alcohol aromatic ring. We experimentally confirm products identified in past work, including products predicted in a theoretical study (Wang, 2015). We also quantify the branching to HBA, benzaldehyde, phenol, and 5-hydroxy-4-oxo-2-pentenal. We find the branching fraction for HBA, the primary oxidation product, is ~ 36%. Benzaldehyde has a branching fraction of ~ 21%.

2 Methods

Chamber experiments were conducted to elucidate the chemical mechanism of benzyl alcohol oxidation via OH. First-generation oxidation products were used to identify important pathways to SOA formation. Two set-ups were used to investigate this chemistry: 1.) Gas-phase experiments to determine the branching fractions and gas-phase oxidation chemistry; and 2.) particle-phase experiments to measure the SOA yields of the primary benzyl alcohol oxidation products.

2.1 Experimental Design

Gas-phase experiments were conducted in a ~ 0.8 m^3 FEP Teflon-walled environmental chamber, henceforth referred to as Chamber G. Chamber G was filled and evacuated multiple times with purified air prior to experiments. Particle-phase experiments were conducted in a 19 m^3 FEP Teflon-walled environmental chamber (henceforth referred to as Chamber P) which was continuously flushed for > 24 h prior to experiments. All experiments were run at room temperature (~ 22°C), low relative humidity (< 10% RH), and ambient pressure (~ 1 atm). Benzyl alcohol (Sigma Millipore, ReagentPlus ≥ 99%) and benzalde-

hyde (Sigma Millipore, ReagentPlus ≥ 99%) were injected into the chamber by flowing warm air over a measured amount of precursor deposited on a Pall Teflon filter. For gas-phase experiments, o-hydroxybenzyl alcohol (o-HBA) (Sigma Millipore 99%) was injected similarly. Because o-HBA is a relatively low-volatility compound, in order to achieve sufficiently

60 high concentrations in Chamber P for particle-phase experiments, o-HBA was dissolved in milliQ water and injected by bubbling purified air through the solution.

For the high NO gas-phase experiments G2 and G4, methyl nitrite was used as the oxidant precursor. Methyl nitrite was added to the reactor by measuring the pressure of methyl nitrite into an evacuated round-bottom bulb and back-filling the remainder of the bulb volume with nitrogen. NO (1993 ± 20 ppm NO in N_2, Matheson) was prepared in a similar manner.

65 For high NO, particle-phase experiments, NO (506.9 ± 10 ppm NO in N_2) was injected using a mass-flow controller (Sierra Instruments).

In experiments G1, G3, G5, P1, and P2, hydrogen peroxide (H_2O_2) (Sigma Millipore, 50 wt% in H_2O stabilized) was used as the OH precursor by injecting a known mass (G1, G3, and G5) or volumen (P1 and P2) into a glass bulb and flowing purified air over the liquid droplets to add to the reactor. In particle-phase experiments, the H_2O_2 was heated in a water bath ($\sim 42°C$)

70 during injection.

All particle-phase experiments were seeded using a sonicated solution of 0.06 M ammonium sulfate (($NH_4)_2SO_4$). During injection, the seed solution was run through a soft x-ray charge conditioner (TSI Model 3088). In all experiments, ~ 1 h was allowed after all injections were completed and before the lights were turned on to allow for mixing and collection of adequate background data. In particle-phase experiments, this time was also used to confirm previously calculated chamber wall loss

75 parameters (Charan et al., 2018).

Ultraviolet (UV) broadband lights centered around ~ 350 nm were used as the light source for photooxidation (Light Sources, Inc.); oxidation duration was determined so that $\sim 10\%$ of the precursor was reacted in gas-phase reactions. The j_{NO_2} and j_{CH_3ONO} for Chamber G are 4.4×10^{-3} s^{-1} and 1.1×10^{-3} s^{-1}, respectively. The j_{NO_2} and $j_{H_2O_2}$ of Chamber P are measured to be 4.4×10^{-3} s^{-1} and 3.2×10^{-6} s^{-1}, respectively, using methods described elsewhere (Zafonte

80 et al., 1977). Additional information about the oxidants is found in Appendix A. Photooxidation was carried out for particle-phase experiments for > 6 h. This oxidation time corresponds to about $50 - 100\%$ reaction of the initial VOC and is congruent with reaction times in the benzyl alcohol studies in (Charan et al., 2020). A summary of experiments can be found in Table 1.

Table 1. Experimental Summary.

Expt. #	VOC	[VOC] (ppb)	[NO] (ppb)	Oxidant	[Oxidant] (ppb)
			Gas-phase experiments		
G1	Benzyl alcohol	539	1,000	H_2O_2	2,000
G2	Benzyl alcohol	46	500	CH_3ONO	300
G3	Benzyl alcohol	523	50	H_2O_2	2,000
G4	Benzyl alcohol	60	44	CH_3ONO	370
G5	Benzyl alcohol	538	0	H_2O_2	2,000
			Particle-phase experiments		
P1	Hydroxybenzyl alcohol	12	160	H_2O_2	2,000
P2	Benzaldehyde	82	71	H_2O_2	2,000

2.2 Instrumentation

In the particle-phase experiments, NO and NO_2 were monitored using a commercially available Teledyne T200 NO_x monitor. Temperature and RH were measured by a Vaisala HMM211 probe. In gas-phase experiments, NO_x was monitored using commercially available Teledyne M200EU NO_x monitor. Additional instrumentation used in gas-phase and particle-phase experiments is described in the following sections.

2.2.1 Particle Mass Detection

Particle size distribution was monitored using a custom-built scanning mobility particle sizer (SMPS) which uses a commercially available TSI 3081 differential mobility analyzer (DMA) and a TSI 3010 condensation particle counter (CPC) (Mai, 2018). Prior to the DMA inlet, a soft x-ray charger provided a known charge-distribution. Wall loss corrections and subsequent SOA yields were calculated based on work and model development explained in Charan et al. (2018) and Huang et al. (2018), and detailed more specifically for these experiments in Charan et al. (2020). SOA yields were calculated based on a ratio of the mass of the VOC precursor reacted and the mass of the SOA formed:

$$Y = \frac{\Delta SOA}{\Delta VOC \, precursor} \tag{1}$$

Here, ΔSOA is the change in the aerosol mass concentration while accounting for any aerosol loss to the chamber walls. Aerosol density was assumed to be 1.04 g cm^{-3} based on past work on benzyl alcohol (Charan et al., 2020; Li and Cocker, 2018).

2.2.2 Gas-Phase Detection

A chemical ionization triple quadrupole mass spectrometer (CIMS) with a CF_3O^- reagent ion was used to monitor gas-phase compounds in particle-phase experiments. This set up has been described in detail elsewhere (Schwantes et al., 2017). In brief, the CIMS operates by reacting with the gas-phase compounds in the sample that have an electron affinity sufficient to bind with the reagent ion cluster (CF_3O^-). Sampled compounds that are acidic may also transfer a fluoride ion (F^-). The sample is then detected by a Varian 1200 triple quadrupole mass analyzer which measures masses from m/z = 50 to 330. A custom-built inlet to the CIMS was set at a constant temperature, 25°C.

Benzaldehyde, one of the primary products of benzyl alcohol OH oxidation, is not detectable using the CF_3O^- CIMS. Thus an HP 6890N gas chromatograph with a flame ionization detector (GC-FID) was used in in experiments G1, G3, G5, P1, and P2 to detect benzaldehyde. Experiments were run with a DB5 column. Information on the temperature profile and GC operation can be found in Appendix C.

In gas-phase experiments in Chamber G, the GC-CIMS was used to monitor the gas phase precursors and subsequent photooxidation products. This experimental setup is described in detail elsewhere (Vasquez et al., 2018; Xu et al., 2020) Here,

the GC-CIMS was operated in negative mode using CF_3O^-, and for experiments G2 and G4, in positive mode using NO^+. The chemistry involving CF_3O^- is described previously and detailed in Appendix B (Vasquez et al., 2018; Crounse et al., 2006). In positive mode, NO^+ complexes with less acidic compounds and can be detected at $[M+NO^+]$ (also described further in Appendix B). A 2 m Restek RTX-1701 column was used for all experiments for better chromatographic resolution of certain isomers. GC samples were cryogenically trapped at -20°C on the column. Additional information on the GC-CIMS operation is in Appendix C.

2.2.3 Calibrations

The sensitivities for analytes in the GC-CIMS were generally determined from prepared standards and quantified using Fourier transform infrared (FTIR) spectroscopy. The GC-FID and the CIMS in experiments P1 - P2 were calibrated by injecting the analyte of interest into a ~ 100L Teflon pillow bag using the same injection method as described for Chamber G. The sample was then measured via a FTIR spectrometer with a pathlength of 19 cm. Reference FTIR spectra from the Pacific Northwest National Laboratory (PNNL) database were used to tabulate cross sections and determine exact concentrations (Schwantes et al., 2017). The pillow bag was then diluted using dry N_2 and sampled to determine the instrumental sensitivity (Xu et al., 2019).

Several substrates involved in this study are relatively non-volatile, leading to challenges with quantitative transfer into and out of the FTIR cell. Therefore some of the GC-CIMS sensitivities were determined using calculated polarizabilities and dipole moments to determine the ion-molecule collision rates of the analytes with the reagent ion relative to the collision rates with reference calibrants (Su and Chesnavich, 1982; Garden et al., 2009). Additional information on this procedure can be found in Appendix B.

2.3 Corrections

2.3.1 Vapor-wall Loss

Vapor wall loss was examined by sampling benzyl alcohol (and products) prior to oxidation and post-oxidation. Vapor wall loss periods were as long as or on timescales with similar orders of magnitude to the oxidation periods. During these sample periods, the signal of oxidation products ~~remains~~ remained stable. Thus, no vapor-wall loss correction ~~is~~ was applied. This is congruent with past work on quantifying benzyl alcohol products, as well as other work quantifying first-generation gas-phase products, which typically considered gas-phase wall loss to be negligible (Charan et al., 2020; Jaoui et al., 2023; Bernard et al., 2013; Harrison and Wells, 2009).

2.3.2 Secondary Chemistry

Oxidation products of benzyl alcohol react as they are ~~formed - for~~ formed—for some of the oxidation products, their rate coefficient for reaction with OH is faster than benzyl alcohol. These secondary losses were accounted for in estimating the branching fractions of benzyl alcohol products which are reported in Table 4. Branching fractions (BF) were calculated as:

$$BF = Y \times CF \tag{2}$$

The gas-phase, time-dependent yield (Y) is calculated as the amount of oxidation product formed divided by the amount of precursor reacted. To solve for the correction factor (CF), a constant [OH] is assumed for the time-dependent product concentration, which can be described as:

$$[\text{Product}]_t = [\text{BA}]_0 \times \frac{Y \times k_{\text{BA}}}{k_{\text{BA}} - k_{\text{Product}}} \times [e^{-k_{\text{Product}}[\text{OH}]t} - e^{-k_{\text{BA}}[\text{OH}]t}] \tag{3}$$

The time-dependent concentration of benzyl alcohol is described as:

$$[\text{BA}]_t = [\text{BA}]_0 \times e^{-k_{\text{BA}}[\text{OH}]t} \tag{4}$$

Therefore, CF is defined as:

$$CF = \frac{k_{BA} - k_{product}}{k_{BA}} \times \frac{1 - [BA]_t/[BA]_0}{([BA]_t/[BA]_0)^{k_{product}/k_{BA}} - ([BA]_t/[BA]_0)} \tag{5}$$

The kinetic rate constants used to solve for Eq. 5 are found in Table 2. This correction factor is described elsewhere in greater detail (Atkinson et al., 1982). The correction factors are presented in Table 3.

Table 2. Kinetic rate constants used to determine the correction factors for branching fraction calculations.

Compound	k_{OH} ($cm^3 molec^{-1} s^{-1}$)
Benzyl alcohol	$(2.8 \pm 0.7) \times 10^{-11}$*
Benzaldehyde	$(1.29 \pm 0.32) \times 10^{-11}$†
Phenol	$(2.83 \pm 0.57) \times 10^{-11}$††
Butenedial	$(3.45 \pm 0.34) \times 10^{-11}$**
Catechol	$(1.04 \pm 0.21) \times 10^{-10}$***
HBA	$(5.59 \pm 2.2) \times 10^{-11}$‡

*Harrison and Wells (2009) and Bernard et al. (2013) † Calvert et al. (2002). †† Rinke and Zetzsch (1984). ** Martín et al. (2013). *** (Olariu et al., 2000). Note that for 5-hydroxy-4-oxo-2-pentenal, the k_{OH} for butenedial is used to calculate the correction factor. ‡Calculated in the present work.

The time traces for HBA and catechol are consistent with the rapid rate of reaction of HBA with OH, which produces catechol in high yield. This was previously reported by Bernard et al. (2013). Because the kinetics of OH with HBA are unknown, we estimate k_{OH+HBA} using the kinetic rate constant of catechol (Appendix H).

Compound	Correction Factor
HBA	1.4
Benzaldehyde	1.1
5-hydroxy-4-oxo-2-pentenal	1.2
Phenol	1.2

Table 3. Calculated correction factors based on Eq. 5, averaged over all experiments.

Table 4. Branching Fraction Results of Gas-Phase Experiments

Experiment	Hydroxybenzyl Alcohol	Benzaldehyde	5-hydroxy-4-oxo-2-pentenal	Phenol
1,000 ppb NO	$(30 \pm 14)\%$	$(22 \pm 6.0)\%$	$(4.0 \pm 1.6)\%$	$(1.3 \pm 0.58)\%$
500 ppb NO	$(40 \pm 20)\%$	$(19 \pm 12)\%$	$(8.8 \pm 2.7)\%$	$(4.2 \pm 1.9)\%$
50 ppb NO	$(37 \pm 19)\%$	$(21 \pm 6.0)\%$	$(8.6 \pm 3.0)\%$	$(2.6 \pm 1.2)\%$
44 ppb NO	$(39 \pm 20)\%$	$(31 \pm 20)\%$	$(5.9 \pm 2.3)\%$	$(1.2 \pm 0.58)\%$
0 ppb NO	$(34 \pm 17)\%$	$(14 \pm 4.0)\%$	$(3.4 \pm 1.4)\%$	$(1.3 \pm 0.58)\%$
Mean	$(36 \pm 18)\%$	$(21 \pm 10)\%$	$(5.5 \pm 1.9)\%$	$(2.1 \pm 0.97)\%$

3 Results and Discussion

3.1 Gas-Phase branching fractions

Gas-phase products were identified in Experiments G1-3 (Table 4). The secondary losses of first generation products were
minimized by limiting the reaction of benzyl alcohol to ~ 10%. The oxidation of benzyl alcohol forms C7 products, such
as HBA and benzaldehyde. Additionally, we observed C6 (products such as phenol), as well as ring-opening products (such
as 5-hydroxy-4-oxo-2-pentenal). A list of products and their corresponding CIMS chemistry can be found in Appendix D.
Together, these products account for $65 \pm 32\%$ of the loss of benzyl alcohol. The lack of mass closure may reflect the impact
of the endo-cyclization route that is known to result in a large diversity of products (Xu et al., 2020) many of which may be
unmeasureable with CF_3O^- CIMS or have very low vapor pressure, likely yielding aerosol (see Particle-Phase Results).

3.1.1 Hydroxybenzyl Alcohol and Benzaldehyde

Here, we quantify the branching fractions of the primary benzyl alcohol oxidation products, HBA and benzaldehyde, under a
range of NO concentrations. Previous studies of benzyl alcohol oxidation were generally performed under high NO conditions.
Thus, our interest in understanding the extent to which NO affects benzyl alcohol chemistry.

While HBA is not currently included in the Master Chemical Mechanism (MCM) scheme (Jenkin et al., 2003; Bloss et al.,
2005), its formation is predicted and identified in past work on benzyl alcohol kinetics and mechanisms (Calvert et al., 2002;
Bernard et al., 2013; Wang, 2015; Bloss et al., 2005; Jenkin et al., 2003). HBA forms via the addition of the OH radical
to the aromatic ring. This leads to a radical intermediate which is stabilized by the electron delocalization of the remaining

conjugated system. Subsequent abstraction of hydrogen by oxygen restores the aromaticity. We calculated the amount of HBA formed from benzyl alcohol oxidation from the gas-phase experiments conducted in Chamber G (Experiments G1 – G5 in Table 1). We find the branching fraction of HBA to be invariant with [NO]. By averaging over all experiments and accounting for systematic error, we estimate the averaged branching fraction of HBA to be $(36 \pm 18)\%$. The primary oxidation product of HBA appears to be catechol (Appendix H). See Section 3.1.2 for a more detailed discussion of how C6 oxidation compounds are formed. Dihydroxy benzyl alcohol was observed in modest quantities, but given its low vapor pressure we are not able to accurately measure the yield. We also observed masses that corresponded to fragmentation products observed in past studies or believed to form via theoretical calculations such as hydroxyoxopropanal (Harrison and Wells, 2009; Wang, 2015; Jaoui et al., 2023). The mechanism for HBA formation and subsequent chemistry can be found in Figure ~~??~~1. This mechanism is based on observed compounds in the present study as well as ~~well as~~ our understanding of aromatic systems in general. An additional summary of compounds detected can be found in Appendix D.
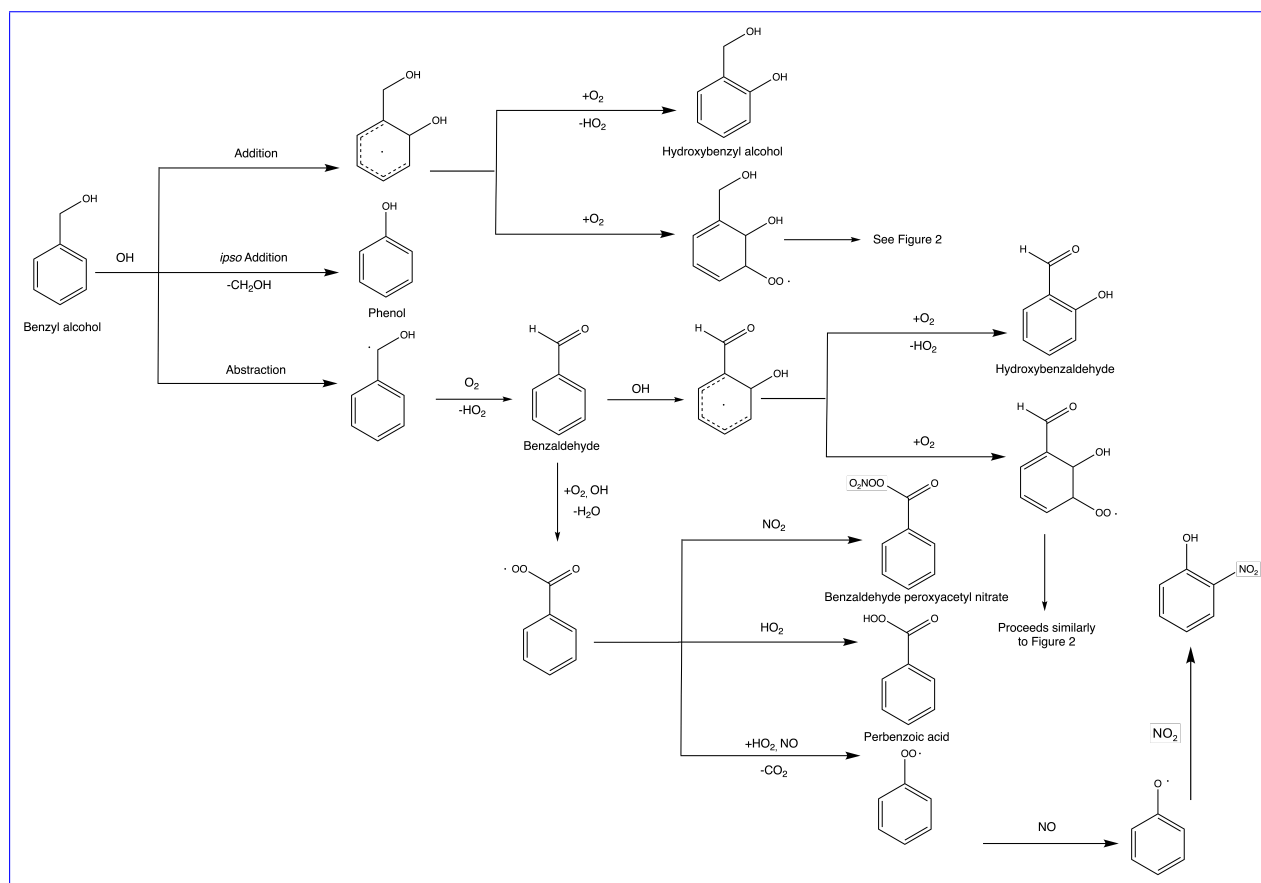
Figure 1. Primary reactive pathways for OH-initiated oxidation of benzyl alcohol.

Benzaldehyde forms via initial hydrogen abstraction from the CH_2OH group followed by addition of O_2 and subsequent loss of HO_2. Benzaldehyde was measured via NO^+ CIMS in experiments G2 and G4 and via GC-FID in experiments G1, G3, and

G5. The NO$^+$ signal is highly water-dependent and therefore less stable than the CF$_3$O$^-$ signal. However, the benzaldehyde branching fraction using the NO$^+$ and GC-FID are in reasonable agreement. We report an averaged branching fraction of $(21\pm10)\%$ under high and low NO conditions, consistent with the expectation that this channel should not have NO dependence when NO is less than several ppm (Allen et al., 2018). Consistent with our findings, others have quantified the branching fraction to benzaldehyde of 25% (Bernard et al., 2013). Oxidation of benzaldehyde by OH can go on to form other closed shell products such as benzyl hydroperoxy and benzaldehyde peroxyacetyl nitrate (Calvert et al., 2002). We observe that the oxidation of benzaldehyde by OH also produces hydroxy benzaldehyde following chemistry analogous to the formation of HBA from benzyl alcohol.

3.1.2 C6 Compounds

~~A previous study~~ Previous studies of the chemical composition of the SOA formed via OH oxidation of benzyl alcohol observed C6 compounds, such as nitrocatechol (Charan et al., 2020; Jaoui et al., 2023). In the present study, we observed nitrocatechol as well as other C6 compounds such as phenol and catechol. Past work has proposed one of two ways to form C6 products. Schwantes et al. (2017) found that C6 products, such as nitrocatechol, can form from the ~~loss of CH$_2$O from benzaldehyde following OH addition (Schwantes et al., 2017). Further reaction with O$_2$ leads to phenol. Other C6 products may also form via hydrogen~~ OH abstraction from the CH$_2$O group ~~in benzaldehyde and subsequenct loss of CO$_2$. Wang (2015) predicted low yields of phenol via decomposition of the HBA radical adduct~~. The second proposed mechanism via theoretical work done by Wang (2015), suggests that formation of C6 compounds, such as phenol, can occur via OH addition to the ipso site of benzyl alcohol. The ipso radical intermediate can then decompose to form phenol ~~and ·CH$_2$OH which will react with O$_2$ to form formaldehyde~~. However, Wang estimated the barrier to this decomposition was too high for significant formation of phenol. ~~In~~ Indeed, in the present study we observed initial branching fractions of phenol $< 5\%$. We also observed that the branching fraction of phenol decreases with decreasing NO, consistent with past studies showing the mechanism for phenol formation depends on NO mixing ratio (Xu et al., 2020). Both mechanisms to C6 formation described in this section are illustrated in Figure 1.

We ~~observed~~ also observed many C6 ~~compounds in both gas-phase~~ products in the aerosol phase. Phenol, catechol, and ~~particle-phase experiments. Phenol~~ and other C6 aromatic compounds react rapidly with OH to form other oxygenated aromatic compounds ($\leq 2.7 \times 10^{-11}$ cm^{3}molecule^{-1}s^{-1}) (Calvert et al., 2002). We ~~observed many~~ hypothesize many of the C6 ~~products in the aerosol~~, compounds we observed in aerosol experiments are likely oxidation products of catechol. ~~Wang (2015) also predicts a considerable yield of nitroaromatics. In high NO conditions, we observed nitrophenol in gas-phase and particle-phase experiments. Furthermore, in past work, nitrocatechol is identified as an important compound in the chemical composition of aerosol formed from benzyl alcohol oxidation (Charan et al., 2020).~~

3.2 Particle-Phase Results

We estimate the relative contributions of HBA and benzaldehyde to benzyl alcohol SOA formation by conducting individual SOA yield experiments using HBA and benzaldehyde as the VOC precursors. Conditions for SOA experiments were selected
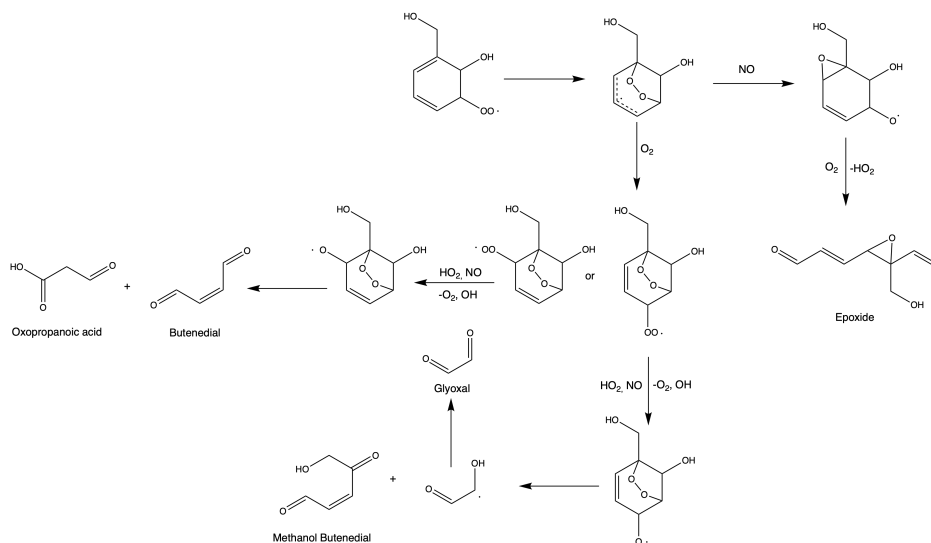
Figure 2. Following addition of OH to the aromatic ring, a bicyclic intermediate can form which can eventually fragment. Here, we detect products with masses congruent with both the 5-hydroxy-4-oxo-2-pentenal and epoxide products.

to match those of the benzyl alcohol SOA yield experiments in Charan et al. (2020). In brief, experiments were conducted with ~ 80 ppb of initial NO, ~ 80 ppb of VOC precursor, and ~ 1×10^4 cm^{-3} inorganic seed aerosol. SOA yield results were calculated using two treatments: one where the proportionality factor, ω, was set to unity and another in which ω=0. In the ω=0 case, oxidation products with a sufficiently low vapor pressure to condense were assumed to do so only on suspended particles and not on particles that had deposited on the chamber walls (Weitkamp et al., 2007). When ω=1, on the other hand, condensable oxidation products and particles deposited on the chamber walls during the experiment were assumed to be in equilibrium with one another (Weitkamp et al., 2007).

Figure 3 shows results for SOA yield experiments using benzaldehyde and HBA. Note the OH exposures for benzaldehyde and HBA in these experiments were approximately 2.8×10^{10} molecule s cm^{-3} and 1.4×10^{10} molecule s cm^{-3}, respectively, which corresponds to ~ 26 min to 52 min of OH exposure on a typical Los Angeles summer day (Appendix F) (Griffith et al., 2016). Both experiments were allowed to react for the same amount of time, ~ 350 minutes, to compare to the SOA yield experiments conducted in Charan et al. (2020). Therefore, we report the SOA yields of HBA and benzaldehyde at t = 350 mins (SOAY$_{350\text{mins}}$), rather than at an equilibrium point. At the upper bound, (ω = 1), SOAY$_{350\text{mins}}$ of HBA is ~~$(87 \pm 9)\%$~~ $(82 \pm 9)\%$ and at the lower bound (ω = 0), SOAY$_{350\text{mins}}$ of HBA is $(69 \pm 9)\%$. For benzaldehyde, we report an upper bound of SOAY$_{350\text{mins}}$ $(67 \pm 17)\%$ and a lower bound of $(46 \pm 17)\%$. While comparing SOAY$_{350\text{mins}}$ is helpful in determining which pathways (addition versus abstraction) contribute to the high SOA yield of benzyl alcohol, this value does not necessarily inform atmospherically relevant SOA yields of benzaldehyde and HBA as inputs for models because modeled reaction time and conditions may not exactly match experimental ones. Therefore, we report the parameterized fit of the SOA yields as a

function of absorbing organic mass concentration (M). In either case, it is clear that the subsequent oxidation of benzaldehyde and HBA contribute significantly to the total SOA yield observed in Charan et al. (2022).
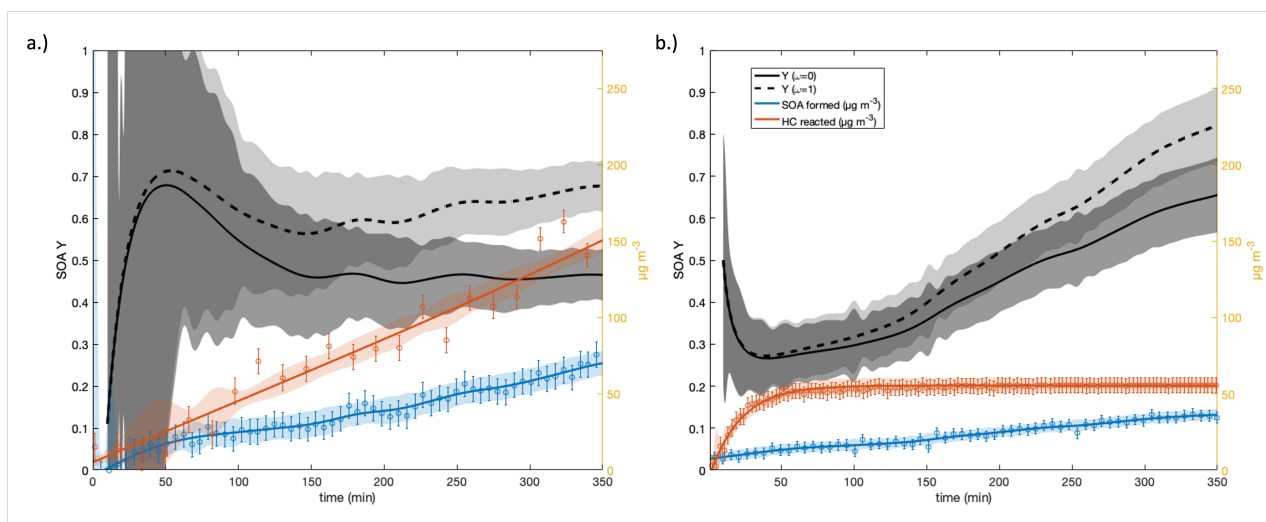

Figure 3. Wall-loss corrected SOA yields of benzaldehyde (a) and HBA (b). Solid yields are calculated assuming ω is zero. Dotted yields are calculated assuming ω equals unity. Red data are the amount of VOC precursor reacted in $\mu g\ m^{-3}$. Data displayed in blue are SOA formed in $\mu g\ m^{-3}$. Note that the first 10 minutes of SOA yield data are excluded because of the relatively low sensitivity and thus high errors in detecting the amount of hydrocarbon reacted and SOA formed at the start of an experiment.

240   We follow a one-product parameterization method that follows the multiple parameterization described in Odum et al. (1996) where,

$$Y = M_o \times \sum_{i}^{n} \frac{\alpha_i \times K_{om,i}}{1 + K_{om,i} \times M_o} \tag{6}$$

Here K_{om} is the partitioning coefficient and α is a constant relating the total concentration of products formed with the amount of organic gas-phase mass reacted. Two parameters were used to fit the present data. The parameters in Equation 6

245   were chosen by minimizing the least square fit to the data. Results for benzaldehyde SOA yield are graphed in Figure 4 for $i = 2$, ($\alpha_{[i=1]} = 0.64$ and $\alpha_{[i=2]} = 0.64$. $K_{om[i=1]} = 0.17$ and $K_{om[i=2]} = 0.73$). For HBA, this approach becomes more complicated. The Odum et al. approach uses the steady state approximation (SSA) which states that the derivative of the concentration of an intermediate species appears to be zero. In other words, we assumed an approximately steady state of first-generation oxidation products which are reacting at roughly the same rate as their formation. The rates of reaction of HBA and subsequent oxidation

250   products were likely unequal because the HBA reacts away early in the experiment; therefore, the SSA was not a sufficient approximation and so, we did not use the two-parameter Odum et al. fitting for HBA.

At t = 350 mins, unreacted benzaldehyde remained in the chamber whereas all of the HBA reacted within the first hour of the experiment. This may indicate that the SOA formed in the benzaldehyde experiments is from the very rapid chemistry of
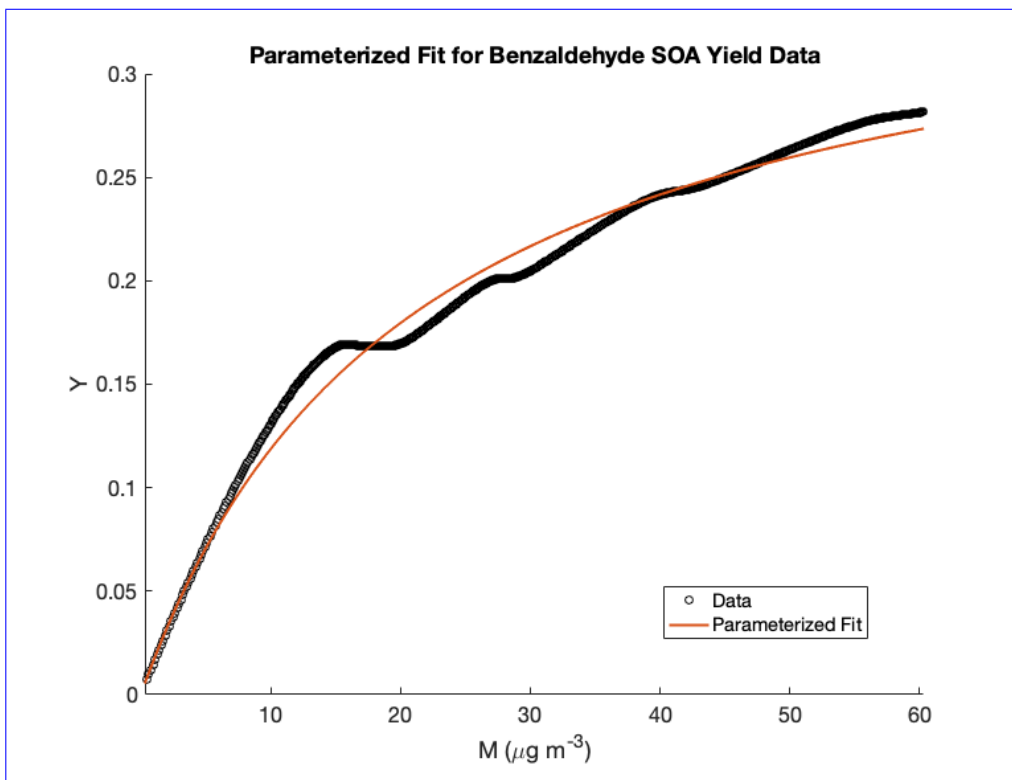
Figure 4. Parameterization of SOA yield data as a function of organic mass reacted. Because SOA yields did not stabilize in these experiments, parameterization can be useful in contextualizing SOA yields under atmospherically relevant conditions.

subsequent generation oxidation products, as is the case with toluene. In the HBA experiments, most of the SOA is likely also generated from the oxidation of later-generation products, such as catechol.

HBA and benzaldehyde both exhibit potential for high SOA yields. HBA may have a slightly higher SOA yield than benzaldehyde and a large branching fraction from benzyl alcohol oxidation, therefore HBA contributes significantly to the large measured SOA yield of benzyl alcohol in our experiments. In aromatic oxidation chemistry, addition of electron-donating groups (such as OH) lowers the barrier of reaction for additional OH chemistry (Calvert et al., 2002). In previously studied aromatic systems, adding electron-donating substituent groups can increase reactivity with OH (Calvert et al., 2002). In the benzyl alcohol system, after every subsequent reaction with the OH radical, we anticipate the kinetics of HBA quickly lead to low-volatility, highly-oxygenated products that readily partition into aerosol. The rapid reaction of HBA leads catechol and other products that react quickly with OH.

3.3   Comparison With Past Work

Past studies have detected HBA and benzaldehyde from the oxidation of benzyl alcohol (Wang, 2015; Bernard et al., 2013; Harrison and Wells, 2009). We estimate the branching fraction to HBA of $(36 \pm 18)\%$. In comparison, Wang (2015) calculated

o-HBA branching of 11% using theoretical methods, while Bernard and coworkers estimated the branching fraction is 21%. The differences with Bernard et al. likely reflects the challenges of quantifying HBA and accounting for its very fast reactivity.

We observed only one isomer of HBA which we assume to be the *ortho* product. This assignment is based on past work that suggests the *ortho* position is a major product in aromatic oxidation chemistry by OH (Harrison and Wells, 2009; **?**; Baltaretu et al., 2009). Similarly, Wang (2015) predicted a single stable isomer of HBA, *ortho*. If additional HBA isomers existed in our system, it is likely they would have eluted at higher temperatures than were allowed by the current GC temperature profiles and were therefore undetected. However, secondary isomer formation is typically considered to be minor in other aromatic systems (**?**Baltaretu et al., 2009).

Bernard et al. (2013) also reported a benzaldehyde yield of $(25\pm4)\%$ (which was used as input to the computations performed in Wang 2015), while Harrison and Wells report a yield of 24% (no error provided) (Bernard et al., 2013; Wang, 2015; Harrison and Wells, 2009). We report a benzladehyde averaged branching fraction of $(21\pm10)\%$, in close agreement with these studies.

4 Conclusions

Benzyl alcohol oxidizes via OH to primarily form HBA and benzaldehyde. Significant additional chemistry occurred via endo-cylization following addition of oxygen to fragmentation products such as 5-hydroxy-4-oxo-2-pentenal and butadiene. We found that [NO] does not affect product yields for HBA, benzaldehyde, or 5-hydroxy-4-oxo-2-pentenal. HBA was the dominant first-generation product with a branching fraction of $\sim 36\%$ over a range of NO conditions. The branching fraction of benzaldehyde is estimated to be $\sim 21\%$.

Both HBA and benzaldehyde go on to form highly oxygenated gas-phase products. HBA oxidation leads to the formation of catechol and dihydroxybenzyl alcohol. Similarly, benzaldehyde oxidation forms products such as dihydroxy benzoic acid. These products indicate that subsequent OH addition to the aromatic ring occur in both pathways. Both the addition and abstraction routes may also contribute to the formation of C6 products.

Aerosol yield studies using HBA and benzaldehyde as the precursors suggested that the HBA pathway is a very important contributor to the high SOA yields observed in benzyl alcohol oxidation. HBA is quickly oxidized by OH to form catechol and subsequently to low-volatility products which rapidly partition to the particle phase, thus contributing to the high SOA yield of benzyl alcohol. Though VCPs have been identified as increasingly important to SOA formation, key VOC components of VCPs remain uncharacterized. Products from benzyl alcohol oxidation via OH were identified here, elucidating its fast reactivity and high aerosol mass yields.

Appendix A: Experimental Conditions

CH_3ONO (synthesized following Taylor et al. (1980)), and NO (1993±20 ppmv, Matheson) were injected into the Chamber G (~ 800 L) in a similar fashion. The analyte is introduced to an evacuated 0.5 L glass bulb and is serially diluted with N_2 until the desired mixing ratio is achieved. CH_3ONO was quantified via FTIR spectroscopy using tabulated cross section prior to being injected into Chamber G. Ultraviolet lights (8 bulbs Sylvania F40/350BL 40 W) centered around 350 nm were used. The measured j_{CH3ONO} and inferred j_{NO2} from these lights are $1.1 \times 10^{-3} s^{-1}$ and $4.4 \times 10^{-3} s^{-1}$, respectively for Chamber G.

Appendix B: CIMS Calibration and Instrument Sensitivity

CF_3O^- ions are produced by flowing the reagent ion source (CF_3OOCF_3 through a radioactive source (^{210}Po). Similarly, $NO^+ \cdot H_2O$ is formed by flowing NO. In negative mode, CF_3O^- ions react with multifunctional organic compounds to form either clusters (Eq. B1) or F^- transfer ions (Eq. B2). CF_3O^- CIMS chemistry is documented extensively in past studies (Vasquez et al., 2018; St. Clair et al., 2010; Crounse et al., 2006).

$$M + CF_3O^- \leftrightarrow M \cdot CF_3O^- \tag{B1}$$

$$M + CF_3O^- \rightarrow M \cdot F^- + CF_2O \tag{B2}$$

In positive mode, $NO^+ \cdot H_2O$ is used (Eq. B3). The $NO^+ \cdot H_2O$ binds to less oxygenated species than CF_3O^- including carbonyls such as benzaldehyde.

$$NO^+ \cdot H_2O + M \rightarrow M \cdot NO^+ + H_2O \tag{B3}$$

The CIMS and GC-FID in experiments in Chamber P were calibrated for benzyl alcohol and benzaldehyde, respectively. The GC-CIMS and GC-FID in experiments in Chamber G were calibrated for phenol and benzaldehyde, respectively. Individual calibrants were injected into a ~ 100 L Teflon pillow bag using the same injection method as described previously. The sample was then measured via a Fourier transform infrared (FTIR) spectrometer with a path length of 19 cm. The reference FTIR spectrum from the Pacific Northwest National Laboratory (PNNL) database was used to tabulate cross sections to determine the exact concentration of the calibrant (Schwantes et al., 2017). The pillow bag was then diluted using dry N_2 and sampled to determine the instrumental sensitivity.

Compound	Average Dipole (D) at 298 K	Polarizability (Å^3)
Phenol	1.828	10.07
Catechol	2.364	10.76
o-Hydroxy benzyl alcohol (o-HBA)	2.109	12.63
p-Hydroxy benzyl alcohol (p-HBA)	1.286	12.76
Benzyl alcohol	1.457	1.780
Z-5OH-4CO-pent-2-enal	3.072	10.55
E-5OH-4CO-pent-2-enal	2.015	10.80
o-Hydroxy benzaldehyde	3.008	12.64

Table B1. Quantum calculations of dipole moments and polarzabilities (at the B3LYP/cc-pVTZ level).

320   Standards of catechol and D5-phenol were prepared from temperature-controlled permeation tubes which were weighed periodically to quantify their emission rates. These standards were then used to calibrate the GC-CIMS for these compounds. The measured and calculated catechol sensitivity (determined relative to phenol) agree within 28% of each other.

     For other less volatile analytes the calculated ion-molecule collision rate was used, relative to phenol (for G1 - G4) or benzyl alcohol (for P1), to estimate the CIMS sensitivities. The sensitivity of o-HBA, p-HBA, 5-hydroxy-4-oxo-2-pentenal, catechol,

325   and benzyl alcohol (G1 - G4) were estimated in this way. Average dipole moments at 298 K and polarizabilities (at B3LYP/cc-pVTZ level) were calculated for all analytes of interest (Table B1). These were used to calculate the ion-collision rate between analytes and reagent ion as described in Su and Chesnavich (1982). Assuming that the clusters are well bound, the sensitivity for a given analyte relative to a reference (here phenol) has been shown to be well represented by the ratio of their ion-molecule collision rates (Murphy et al., 2023).

330   For particle-phase experiments, HBA was calibrated on the CIMS relative to the CIMS sensitivity of benzyl alcohol by comparing the relative GC-CIMS sensitivities of HBA and benzyl alcohol in gas-phase experiments.

Appendix C: GC Operation

In gas-phase experiments, analyte samples were cryogenically trapped for 10 mins on the head of the 20 m, Restek RTX1701 at $\sim -20°C$. The sample then eluted through the GC using a ramp of $10°C/min$ to $55°C$ and then $2.5°C/min$ to $130°C$. The

335   slower ramp rate from $55 - 130°C$ was used because most oxidation products eluted at this time and using a slower ramp ensured relevant products were sufficiently separated. When GC scans were not being taken, the CIMS sampled directly from the reaction chamber.

     For the particle-phase experiments, the GC-FID was run from $40°C$ to $250°$ C with a ramp rate of $50°C/min$. For gas-phase experiments, however, where benzyl alcohol was used as the precursor, we were interested in detecting and quantifying both

340   benzaldehyde and benzyl alcohol. A DB-5 column in the GC-FID was used for all experiments.

Appendix D: Oxidation Products Detected

The following table summarizes masses detected by the GC-CIMS in gas-phase experiments (G1 - G3). While some products were identified using authentic standards, other assignments are based on masses detected and our chemical understanding of this and other aromatic systems.

Appendix E: Estimation of Uncertainty

In gas phase experiments, the major source of error in our calculation of branching ratios comes from the knowledge of the CIMS sensitivity to the analytes measured. A part of the uncertainty comes from propagating the error of phenol calibrated via the permeation tubes since several of the analytes were calibrated relative to phenol. Some uncertainty is also derived from the calculated ion-molecule collision rates which were based on the computationally derived dipole moments and polarizabilities. A smaller part of the reported error is also determined from the standard deviation of signals. This varies from compound to compound and is also dependent on the reagent gas used. As an example, catechol was calibrated both using the permutation tube method and using the computational method. The two calibration factors varied by ~ 28%. Based on this, we estimate the error for the normalized branching fractions to be ~ 45%, congruent with past work using similar experimental setups (Praske et al., 2018; Yu et al., 2023). HBA branching ratios have a slightly higher uncertainty because of our treatment of its secondary chemistry (see Section 2.3.2).

Appendix F: OH Exposure

[OH] was calculated for SOA yield experiments using the kinetic equation:

$$\frac{d[\text{reagent}]}{dt} = -k_{OH}[OH][\text{reagent}] \tag{F1}$$

Here, $\frac{d[\text{reagent}]}{dt}$ was determined by finding the log of the slope of the starting reagent against time. For benzaldehyde, the log of the slope over the entire experiment was used and assuming $k_{OH} = (1.29 \pm 0.32) \times 10^{-11}$ $cm^3 molec^{-1}s^{-1}$. For HBA, the log of the slope for the first 15 min was used to determine [OH] for the experiment, and assuming k_{OH} of HBA = $(5.59 \pm 2.2) \times 10^{-11}$ $cm^3 molec^{-1}s^{-1}$.

Appendix G: Wall-Loss

Particle wall loss was accounted for in SOA yield experiments using methods described in Charan et al. (2020) and Charan et al. (2018). In short, the SOA data were fit by parameterizing the eddy diffusivity coefficient (ke). The mean electric field experienced within the chamber (E) was assumed to be zero because the environmental chambers are enclosed and undisturbed
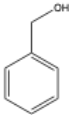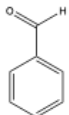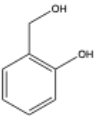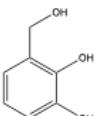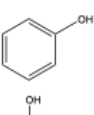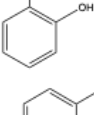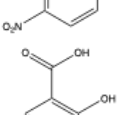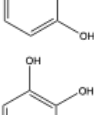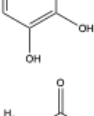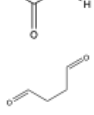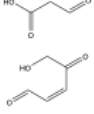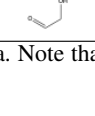
VOC Compound (m/z)	Structure	Formula	Observed m/z and Reagent Ion
Benzyl alcohol (108)		$C_6H_5CH_2OH$	193 (CF_3O^-)
Benzaldehyde (106)		$C_6H_5C(O)$	136 (NO^+)
Hydroxybenzyl alcohol (124)		$C_6H_4OHCH_2OH$	143 (F^-) and 209 (CF_3O^-)
Dihydroxybenzyl alcohol (140)		$C_6H_4OHOHCH_2OH$	225 (CF_3O^-)
Phenol (94)		C_6H_5OH	113 (F^-) and 179 (CF_3O^-)
Catechol (110)		C_6H_4OHOH	129 (F^-) and 195 (CF_3O^-)
Nitrophenol (139)		$C_6H_5NO_3$	158 (F^-)
Dihydroxybenzoic acid (154)		$C_6H_3OHOHC(O)OH$	173 (F^-)
Tetrahydroxy benzene (142)		$C_6H_6O_4$	161 (F^-)
Glyoxal (58)		$C_2H_2O_2$	88 (NO^+)
Butenedial (84)		$C_4H_4O_2$	114 (NO^+)
Oxopropanoic acid (88)		$C_3H_4O_3$	173 (CF_3O^-)
5-hydroxy-4-oxo-2-pentenal (114)		$C_5O_3H_6$	199 (CF_3O^-)
Hydroxyacetaldehyde (60)		$C_2O_2H_4$	145 (CF_3O^-)

Table D1. Compound assignments from CIMS data. Note that several of the compounds listed have many isomeric structures though only one may be listed as an example.
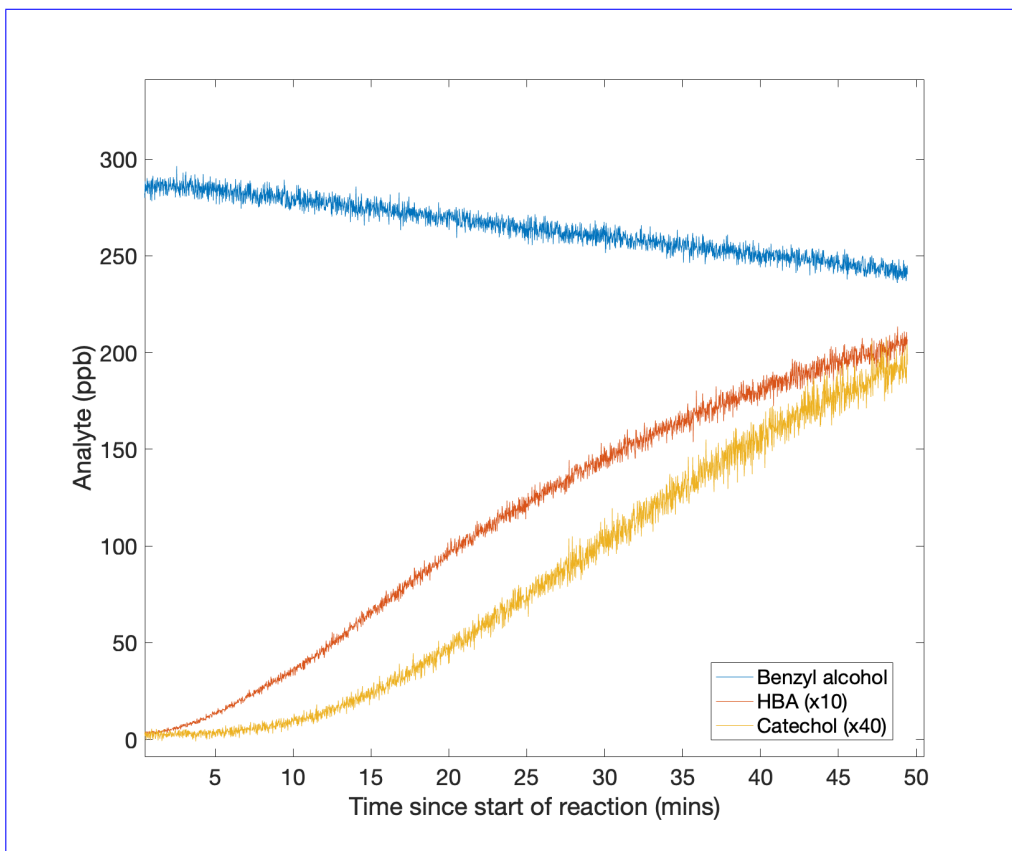
Figure H1. Consistent with a ~~previous study~~ Bernard et al. (~~cite~~2013), catechol is a major oxidation product of hydroxybenzyl alcohol (HBA). Note that the compounds are displayed here as x10 (HBA) and x40 (catechol).

prior to the experiments and therefore have no charge source. For experiment P1, ke = 0.720 was used and for experiment P2, ke = 0.346 was used.

Appendix H: Secondary Chemistry

370   We use the kinetics of cresol to estimate k_{OH+HBA} in order to make secondary chemistry corrections for the branching ratio of HBA. $K_{OH+cresol}$ is used because of its similar structure to HBA. We use a structure additivity correction to account for the abstractable hydrogens of HBA compared to cresol. We find that this rate is broadly consistent with the observed time dependence of HBA and catechol (Figure ~~??~~H1).

Appendix I: Excluded Data

375   One experiment was excluded from the data presented. This gas-phase experiment was run under similar conditions to those reported in the main text and with 0 ppb NO. This experiment was excluded because the relatively low amount of benzyl alcohol reacted resulted in very large uncertainty in the branching fractions of HBA and benzaldehyde.

Author contributions.   RSB: study conceptualization, data collection and analysis, result interpretation, and writing. SMC: Analysis code and writing. JHS: supervision and writing. POW: supervision, result interpretation, and writing.

References

Allen, H. M., Crounse, J. D., Bates, K. H., Teng, A. P., Krawiec-Thayer, M. P., Rivera-Rios, J. C., Keutsch, F. N., St. Clair, J. M., Hanisco, T. F., Møller, K. H., Kjaergaard, H. G., and Wennberg, P. O.: Kinetics and Product Yields of the OH Initiated Oxidation of Hydroxymethyl Hydroperoxide, The Journal of Physical Chemistry A, 122, 6292–6302, https://doi.org/10.1021/acs.jpca.8b04577, 2018.

390 Atkinson, R., Aschmann, S. M., Carter, W. P., Winer, A. M., and Pitts, J. N.: Alkyl nitrate formation from the NO-air photooxidations of C2-C8 n-alkanes, Journal of Physical Chemistry, The, 86:23, 7, https://doi.org/10.1021/j100220a022, 1982.

Baltaretu, C. O., Lichtman, E. I., Hadler, A. B., and Elrod, M. J.: Primary atmospheric oxidation mechanism for toluene, The Journal of Physical Chemistry A, 113, 221–230, https://doi.org/10.1021/jp806841t, 2009.

Bernard, F., Magneron, I., Eyglunent, G., Daële, V., Wallington, T. J., Hurley, M. D., and Mellouki, A.: Atmospheric chemistry
395 of benzyl alcohol: kinetics and mechanism of reaction with OH radicals, Environmental Science & Technology, 47, 3182–3189, https://doi.org/10.1021/es304600z, 2013.

Bloss, C., Wagner, V., Jenkin, M., Volkamer, R., Bloss, W., Lee, J. D., Heard, D. E., Wirtz, K., Martin-Reviejo, M., Rea, G., Wenger, J. C., and Pilling, M. J.: Development of a detailed chemical mechanism (MCMv3.1) for the atmospheric oxidation of aromatic hydrocarbons, Atmospheric Chemistry and Physics, 2005.

400 Burkholder, J. B., Abbatt, J. P. D., Barnes, I., Roberts, J. M., Melamed, M. L., Ammann, M., Bertram, A. K., Cappa, C. D., Carlton, A. G., Carpenter, L. J., Crowley, J. N., Dubowski, Y., George, C., Heard, D. E., Herrmann, H., Keutsch, F. N., Kroll, J. H., McNeill, V. F., Ng, N. L., Nizkorodov, S. A., Orlando, J. J., Percival, C. J., Picquet-Varrault, B., Rudich, Y., Seakins, P. W., Surratt, J. D., Tanimoto, H., Thornton, J. A., Tong, Z., Tyndall, G. S., Wahner, A., Weschler, C. J., Wilson, K. R., and Ziemann, P. J.: The essential role for laboratory studies in atmospheric chemistry, Environmental Science & Technology, 51, 2519–2528, https://doi.org/10.1021/acs.est.6b04947, 2017.

405 Calvert, J. G., Atkinson, Roger, Becker, Karl H., Kamens, Richard M., Seinfeld, J. H., Wallington, Timothy J., and Yarwood, Greg: The mechanism of atmospheric oxidation of aromatic hydrocarbons, Oxford University Press, New York, New York, 2002.

Charan, S. M., Kong, W., Flagan, R. C., and Seinfeld, J. H.: Effect of particle charge on aerosol dynamics in Teflon environmental chambers, Aerosol Science and Technology, 52, 854–871, https://doi.org/10.1080/02786826.2018.1474167, 2018.

Charan, S. M., Buenconsejo, R. S., and Seinfeld, J. H.: Secondary organic aerosol yields from the oxidation of benzyl alcohol, Atmospheric
410 Chemistry and Physics, 20, 13 167–13 190, https://doi.org/10.5194/acp-20-13167-2020, 2020.

Charan, S. M., Huang, Y., Buenconsejo, R. S., Li, Q., Cocker III, D. R., and Seinfeld, J. H.: Secondary organic aerosol formation from the oxidation of decamethylcyclopentasiloxane at atmospherically relevant OH concentrations, Atmospheric Chemistry and Physics, 22, 917–928, https://doi.org/10.5194/acp-22-917-2022, 2022.

Coggon, M. M., Gkatzelis, G. I., McDonald, B. C., Gilman, J. B., Schwantes, R. H., Abuhassan, N., Aikin, K. C., Arend, M. F., Berkoff,
415 T. A., Brown, S. S., Campos, T. L., Dickerson, R. R., Gronoff, G., Hurley, J. F., Isaacman-VanWertz, G., Koss, A. R., Li, M., McKeen, S. A., Moshary, F., Peischl, J., Pospisilova, V., Ren, X., Wilson, A., Wu, Y., Trainer, M., and Warneke, C.: Volatile chemical product emissions enhance ozone and modulate urban chemistry, Proceedings of the National Academy of Sciences, 118, e2026653 118, https://doi.org/10.1073/pnas.2026653118, 2021.

Crounse, J. D., McKinney, K. A., Kwan, A. J., and Wennberg, P. O.: Measurement of gas-phase hydroperoxides by chemical ionization mass
420 spectrometry, Analytical Chemistry, 78, 6726–6732, https://doi.org/10.1021/ac0604235, 2006.

Garden, A. L., Paulot, F., Crounse, J. D., Maxwell-Cameron, I. J., Wennberg, P. O., and Kjaergaard, H. G.: Calculation of conformationally weighted dipole moments useful in ion–molecule collision rate estimates, Chemical Physics Letters, 474, 45–50, https://doi.org/10.1016/j.cplett.2009.04.038, 2009.

Griffith, S. M., Hansen, R. F., Dusanter, S., Michoud, V., Gilman, J. B., Kuster, W. C., Veres, P. R., Graus, M., Gouw, J. A., Roberts, J.,
425   Young, C., Washenfelder, R., Brown, S. S., Thalman, R., Waxman, E., Volkamer, R., Tsai, C., Stutz, J., Flynn, J. H., Grossberg, N., Lefer, B., Alvarez, S. L., Rappenglueck, B., Mielke, L. H., Osthoff, H. D., and Stevens, P. S.: Measurements of hydroxyl and hydroperoxy radicals during CalNex-LA: Model comparisons and radical budgets, Journal of Geophysical Research: Atmospheres, 121, 4211–4232, https://doi.org/10.1002/2015JD024358, 2016.

Harrison, J. C. and Wells, J.: Gas-phase chemistry of benzyl alcohol: Reaction rate constants and products with OH radical and ozone,
430   Atmospheric Environment, 43, 798–804, https://doi.org/10.1016/j.atmosenv.2008.11.001, 2009.

Huang, Y., Zhao, R., Charan, S. M., Kenseth, C. M., Zhang, X., and Seinfeld, J. H.: Unified Theory of Vapor–Wall Mass Transport in Teflon-Walled Environmental Chambers, Environmental Science & Technology, 52, 2134–2142, https://doi.org/10.1021/acs.est.7b05575, 2018.

Jaoui, M., Docherty, K. S., Lewandowski, M., and Kleindienst, T. E.: Yields and molecular composition of gas-phase and secondary organic
435   aerosol from the photooxidation of the volatile consumer product benzyl alcohol: formation of highly oxygenated and hydroxy nitro-aromatic compounds, Atmospheric Chemistry and Physics, 23, 4637–4661, https://doi.org/10.5194/acp-23-4637-2023, 2023.

Jenkin, M., Saunders, S., Wagner, V., and Pilling, M.: Protocol for the development of the Master Chemical Mechanism, MCM v3 (Part B): Tropospheric degradation of aromatic volatile organic compounds, Atmospheric Chemistry and Physics, 2003.

Li, L. and Cocker, D. R.: Molecular structure impacts on secondary organic aerosol formation from glycol ethers, Atmospheric Environment,
440   180, 206–215, https://doi.org/10.1016/j.atmosenv.2017.12.025, 2018.

Mai, H.: Scanning Electrical Mobility Methods for Aerosol Characterization, Ph.D. thesis, California Institute of Technology, 10.7907/9D4H-QS44, 2018.

Martín, P., Cabañas, B., Colmenar, I., Salgado, M. S., Villanueva, F., and Tapia, A.: Reactivity of E-butenedial with the major atmospheric oxidants, Atmospheric Environment, 70, 351–360, https://doi.org/10.1016/j.atmosenv.2013.01.041, 2013.

445   McDonald, B. C., de Gouw, J. A., Gilman, J. B., Jathar, S. H., Akherati, A., Cappa, C. D., Jimenez, J. L., Lee-Taylor, J., Hayes, P. L., McKeen, S. A., Cui, Y. Y., Kim, S.-W., Gentner, D. R., Isaacman-VanWertz, G., Goldstein, A. H., Harley, R. A., Frost, G. J., Roberts, J. M., Ryerson, T. B., and Trainer, M.: Volatile chemical products emerging as largest petrochemical source of urban organic emissions, Science, 359, 760–764, https://doi.org/10.1126/science.aaq0524, 2018.

Murphy, S. E., Crounse, J. D., Møller, K. H., Rezgui, S. P., Hafeman, N. J., Park, J., Kjaergaard, H. G., Stoltz, B. M., and Wennberg, P. O.:
450   Accretion product formation in the self-reaction of ethene-derived hydroxy peroxy radicals, Environmental Science: Atmospheres, 3, 882–893, https://doi.org/10.1039/D3EA00020F, 2023.

Odum, J. R., Hoffmann, T., Bowman, F., Collins, D., Flagan, R. C., and Seinfeld, J. H.: Gas/Particle Partitioning and Secondary Organic Aerosol Yields, Environmental Science & Technology, 30, 2580–2585, https://doi.org/10.1021/es950943+, 1996.

Olariu, R. I., Barnes, I., Becker, K. H., and Klotz, B.: Rate coefficients for the gas-phase reaction of OH radicals with se-
455   lected dihydroxybenzenes and benzoquinones, International Journal of Chemical Kinetics, 32, 696–702, https://doi.org/10.1002/1097-4601(2000)32:11<696::AID-KIN5>3.0.CO;2-N, 2000.

Parker, H. A., Hasheminassab, S., Crounse, J. D., Roehl, C. M., and Wennberg, P. O.: Impacts of Traffic Reductions Associated With COVID-19 on Southern California Air Quality, Geophysical Research Letters, 47, https://doi.org/10.1029/2020GL090164, 2020.

Pennington, E. A., Seltzer, K. M., Murphy, B. N., Qin, M., Seinfeld, J. H., and Pye, H. O. T.: Modeling secondary organic aerosol formation

460   from volatile chemical products, Atmospheric Chemistry and Physics, 21, 18 247–18 261, https://doi.org/10.5194/acp-21-18247-2021, 2021.

Praske, E., Otkjær, R. V., Crounse, J. D., Hethcox, J. C., Stoltz, B. M., Kjaergaard, H. G., and Wennberg, P. O.: Atmospheric autoxidation is increasingly important in urban and suburban North America, Proceedings of the National Academy of Sciences, 115, 64–69, https://doi.org/10.1073/pnas.1715540115, 2018.

465 Rinke, M. and Zetzsch, C.: Rate Constants for the Reactions of OH Radicals with Aromatics: Benzene, Phenol, Aniline, and 1,2,4-Trichlorobenzene, Berichte der Bunsengesellschaft für physikalische Chemie, 88, 55–62, https://doi.org/10.1002/bbpc.19840880114, 1984.

Schwantes, R. H., Schilling, K. A., McVay, R. C., Lignell, H., Coggon, M. M., Zhang, X., Wennberg, P. O., and Seinfeld, J. H.: Formation of highly oxygenated low-volatility products from cresol oxidation, Atmospheric Chemistry and Physics, 17, 3453–3474,

470   https://doi.org/10.5194/acp-17-3453-2017, 2017.

Seinfeld, J. H. and Pandis, S. N.: Atmospheric chemistry and physics: From air pollution to climate change, John Wiley & Sons, Hoboken, New Jersey, third edition edn., 2016.

Seltzer, K. M., Pennington, E., Rao, V., Murphy, B. N., Strum, M., Isaacs, K. K., and Pye, H. O. T.: Reactive organic carbon emissions from volatile chemical products, Atmospheric Chemistry and Physics, 21, 5079–5100, https://doi.org/10.5194/acp-21-5079-2021, 2021.

475 St. Clair, J. M., McCabe, D. C., Crounse, J. D., Steiner, U., and Wennberg, P. O.: Chemical ionization tandem mass spectrometer for the *in situ* measurement of methyl hydrogen peroxide, Review of Scientific Instruments, 81, 094 102, https://doi.org/10.1063/1.3480552, 2010.

Su, T. and Chesnavich, W. J.: Parametrization of the ion-polar molecule collision rate constant by trajectory calculations, The Journal of Chemical Physics, 76, 5183–5185, https://doi.org/10.1063/1.442828, 1982.

Taylor, W., Allston, T., Moscato, M., Fazekas, G., Kozlowski, R., and Takacs, G.: Atmospheric photodissociation lifetimes for nitromethane,

480   methyl nitrite, and methyl nitrate, International Journal of Chemical Kinetics, 12, 231–240, https://doi.org/10.1002/kin.550120404, 1980.

Vasquez, K. T., Allen, H. M., Crounse, J. D., Praske, E., Xu, L., Noelscher, A. C., and Wennberg, P. O.: Low-pressure gas chromatography with chemical ionization mass spectrometry for quantification of multifunctional organic compounds in the atmosphere, Atmospheric Measurement Techniques, 11, 6815–6832, https://doi.org/10.5194/amt-2018-223, 2018.

Wang, L.: The Atmospheric Oxidation Mechanism of Benzyl Alcohol Initiated by OH Radicals: The Addition Channels, ChemPhysChem,

485   16, 1542–1550, https://doi.org/10.1002/cphc.201500012, 2015.

Weitkamp, E. A., Sage, A. M., Pierce, J. R., Donahue, N. M., and Robinson, A. L.: Organic Aerosol Formation from Photochemical Oxidation of Diesel Exhaust in a Smog Chamber, Environmental Science & Technology, 41, 6969–6975, https://doi.org/10.1021/es070193r, 2007.

Xu, L., Møller, K. H., Crounse, J. D., Otkjær, R. V., Kjaergaard, H. G., and Wennberg, P. O.: Unimolecular Reactions of Peroxy Radicals Formed in the Oxidation of alpha-Pinene and beta-Pinene by Hydroxyl Radicals, The Journal of Physical Chemistry A, 123, 1661–1674,

490   https://doi.org/10.1021/acs.jpca.8b11726, 2019.

Xu, L., Møller, K. H., Crounse, J. D., Kjaergaard, H. G., and Wennberg, P. O.: New Insights into the Radical Chemistry and Product Distribution in the OH-Initiated Oxidation of Benzene, Environmental Science & Technology, 54, 13 467–13 477, https://doi.org/10.1021/acs.est.0c04780, 2020.

Yu, H., Møller, K. H., Buenconsejo, R. S., Crounse, J. D., Kjaergaard, H. G., and Wennberg, P. O.: Atmospheric photo-

495   oxidation of 2-ethoxyethanol: autoxidation chemistry of glycol ethers, The Journal of Physical Chemistry A, p. acs.jpca.3c04456, https://doi.org/10.1021/acs.jpca.3c04456, 2023.

Zafonte, L., Rieger, P. L., and Holmes, J. R.: Nitrogen dioxide photolysis in the Los Angeles atmosphere, Environmental Science & Technology, 11, 483–487, https://doi.org/10.1021/es60128a006, 1977.